J Mater Sci: Mater Med (2009) 20:497–505
DOI 10.1007/s10856-008-3612-1

Preparation and characterization of 3D porous ceramic scaffolds based on portland cement for bone tissue engineering

Alexandra A. P. Mansur · Herman S. Mansur

Received: 25 June 2008 / Accepted: 2 October 2008 / Published online: 24 October 2008

Abstract There is a constant need for bone substitutes. This work was focused on developing a porous substrate based on Portland cement with air-voids introduced by outgassing reaction product from lime and aluminum powder. The structures were obtained through two routes of raw-materials and processing. Water absorption and compressive strength measurements and scanning electron microscopy, X-ray diffraction, and Fourier Transformed Infrared Spectroscopy assays were conducted in order to characterize the porous substrates. The substrates have shown pore size structure compatible with bone tissue colonization. Also, the mechanical strength exhibited by the scaffolds fall in the normal ranges for trabecular bone. These characteristics indicate potential use of the developed porous scaffold for bone tissue engineering which was endorsed by in vitro experiments via cell culture.

1 Introduction

There is a constant need for bone substitutes due to severe bone injuries, degenerative diseases, and reconstructive surgery [1–3]. Bone tissue engineering seeks to promote the regeneration of damaged or lost bone tissue through therapies based on a combination of scaffolds, growth factors, and cells [4]. Ideal scaffolds for bone tissue engineering require three-dimensional interconnected porous structures and enough mechanical strength to provide structural support during bone growth and remodeling [5]. In addition, bone substitutes should also possess a bioactive behavior, promoting intense osteointegration and stimulating the growth of bone cells [6].

Previous works [6–10] have shown the potential use of biomaterials based on calcium silicates sintered or hydrated associated with their load bearing capabilities, biocompatibility, and possibility of being produced in situ at room-temperature in the desired shapes and dimensions. Also, calcium silicate substrates can induce the formation of an apatite-like layer in vitro and in vivo increasing the bioactivity of these materials.

Dicalcium silicate ($2CaO \cdot SiO_2$) and tricalcium silicate ($3CaO \cdot SiO_2$) are the major constituents of Portland cement. They possess hydraulic property and spontaneous development of strength towards water [11]. Hydrated Portland cement could be highly cytotoxic due to its alkaline nature [6]. However, under carbonation treatments or by using pozzolanic materials it is possible to counteract this effect by neutralizing the pH of the material resulting in adequate cytocompatibility [6, 9].

The aim of this work was to develop a new three-dimensional bioceramic scaffold for bone tissue repairing based on Portland cement with H_2 as porogen agent product of lime and aluminum powder reaction.

2 Materials and methods

2.1 Scaffolds fabrication and characterization

Portland cement (Camargo Côrrea Cimentos S.A.), lime (Mineração Belocal Ltda.), quartz sand (Precon Industrial S.A.), calcium carbonate (Mineração Fazenda Brasileiro S.A.), silica fume (Camargo Côrrea Cimentos S.A.), and

A. A. P. Mansur · H. S. Mansur (✉)
Department of Metallurgical and Materials Engineering, Federal University of Minas Gerais, Rua Espírito Santo, 35/316-Centro, CEP: 30.160-030 Belo Horizonte, MG, Brazil
e-mail: hmansur@demet.ufmg.br

aluminum powder (Aldoro Indústria de Pós e Pigmentos Metálicos Ltda.) were used to produce the scaffolds. All materials were commercial grade products and their characteristics are summarized in Table 1.

Two routes of raw materials and methods of curing have been used to prepare the scaffolds. In the first (R1), ball-milled quartz was used as filler and, in the second path (R2), silica fume was the choice in order to improve resistance and decrease cement matrix alkalinity related to its pozzolanic activity [12].

After mixing, the slurry was poured into molds in which hydrogen gas was generated by the chemical reaction between fine aluminum powder and lime (according Eqs. 1 and 2) forming small, finely dispersed, air spaces [13]. The materials remain in the mold for the time period needed to ensure the adequate green strength for later demolding and transporting to the final treatment.

$$CaO_{(s)} + H_2O_{(l)} \rightarrow Ca(OH)_{2(aq)} \quad (1)$$

$$6Al_{(s)} + 3Ca(OH)_{2(aq)} + 6H_2O_{(l)} \rightarrow 3CaO \cdot Al_2O_3 \cdot 6H_2O_{(s)} + 3H_{2(g)} \uparrow \quad (2)$$

The foamed green substrates were autoclaved (A) or air cured (NA). Scaffolds obtained through Route 1 were autoclaved (R1_A) and non-autoclaved (R1_NA) while R2 materials were only air cured (R2_NA).

A schematic representation of the whole manufacturing process developed in this work is shown in Fig. 1. Proportions of all compounds were kept constant in the formulations except for water in R2 in which higher water: solids ratio was necessary to obtain similar workability (Patent deposit pending).

Water absorption and compressive strength measurements, besides scanning electron microscopy (SEM), X-ray diffraction (XRD), and Fourier Transformed Infrared Spectroscopy (FTIR) assays, were conducted in order to characterize the porous substrates. Tests and analyses of samples were performed at ages of 28 days.

Water absorption was measured by drying the specimen to constant mass, immersing it in water at (25 ± 3)°C for 72 h, and calculating the mass gained as a percentage of dry mass. Absorption was evaluated on 4 cube specimens ($a = 50$ mm) for each type of substrates.

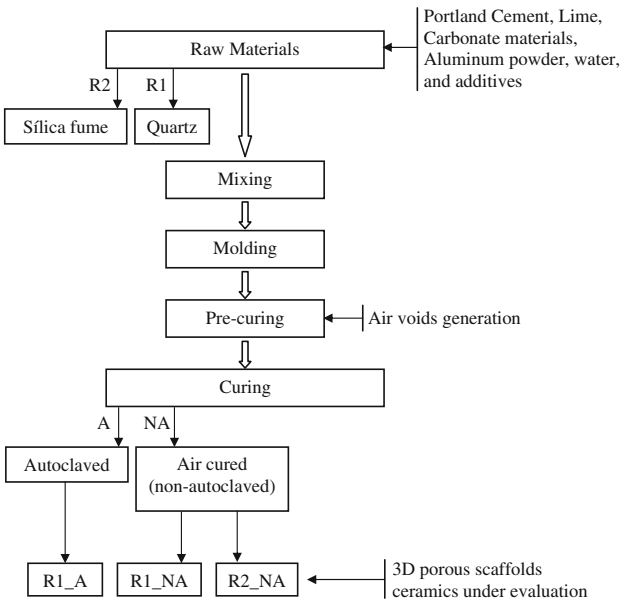

Fig. 1 Schematic representation of ceramic scaffolds manufacturing process

The compressive strength of the R1_A, R1_NA, and R2_NA scaffolds, with the size of 25 × 25 × 50 mm^3 (height) and dried at (60 ± 5)°C/24 h, were determined using a computer-controlled universal testing machine (DL 3000, EMIC) at a crosshead speed of 1.0 mm/min. At least five samples ($n = 5$) of each system were measured and the results averaged.

SEM images were taken from fractured surfaces of substrates with a JSM 6360LV, Jeol/Noran, microscope. Before examination, samples were coated with a thin gold film by sputtering. Images of secondary electrons (SE) were obtained using an accelerating voltage of 15 kV.

The mineralogical phases contained in the samples were determined by means of X-ray diffraction using PW 1710 diffractometer (Philips) with Kα–Cu radiation ($\lambda = 1.5406$ Å) and 0.02° 2θ increment, scanning from

Table 1 Materials used and their characteristics

Material	Particle size Reference	Composition/Purity
Portland cement	Surface area ≥3,000 m^2/kg	Cement type CPV ARI according Brazilian Standard NBR 5733 (similar to Type III ASTM C595)
Lime	Percent retained on 115 mesh screen <3 wt%	CaO ≥80%
Quartz sand	Percent retained on 200 mesh screen <20 wt%	Crystalline SiO_2 >95%
Calcium carbonate	Percent retained on 100 mesh screen <7 wt%	$CaCO_3$ >90%
Silica fume	Surface area ≥2,000 m^2/kg	Amorphous SiO_2 >85%
Aluminum powder	Percent retained on 325 mesh screen <10 wt%	Al >92%

3° e 80° 2θ. The results were compared with the ICDD database. Before XRD analyses, samples were crushed and sieved (#200 mesh).

Powdered and sieved samples (#200 mesh) were analyzed by FTIR spectroscopy with diffuse-reflectance accessory (Perkin-Elmer, Paragon 1000). Samples were placed in a sampling cup and 32 scans were acquired at 2 cm^{-1} resolution with the subtraction of KBr background (4,000–600 cm^{-1}).

2.2 Cytocompatibility, cell viability and bioactivity assays on porous scaffolds

The cytocompatibility was assessed by the reduction of the MTT (3-[4,5-dimetylthiazole-2-yl]-2,5-diphenyltetrazolium bromide) test. VERO cell monolayers were grown in 96-well microtiter plates. Cell proliferation was measured at 2, 4, 6, and 8 days using MTT assay. MTT reagent was added to each sample and incubated at 37°C for 4 h. This latter procedure was also performed simultaneously for the control cells grown on plastic and for hydroxyapatite (HA) used as reference. Absorbance was read on a microplate reader (@ wavelength $\lambda = 595$ nm). The background absorbance produced by wells containing no cells was subtracted from all samples.

Cell viability was also evaluated by spreading and attachment assays in order to examine their morphology, adhesion, and spreading behavior. VERO cells were plated at 6×10^4 density on the macroporous scaffolds after ethylene oxide sterilization. Cell spreading was evaluated by scanning electron microscopy of the specimens after culturing for 2 h. Before microscopy analysis, specimens were fixed with 2% glutaraldehyde for 16 h and dehydrated by passing through a series of alcohol solutions (ethanol-water). Then, they were dried in nitrogen flowing reactor for 4 h and out-gassed in vacuum desiccator for 12 h. Finally, prior to SEM assessment, samples were coated with a thin layer of sputtered Au to make them conductive.

3 Results and discussion

3.1 Scaffolds characterization

Figure 2 shows the typical pore system of the prepared 3D scaffolds. The material structure is characterized by its solid micropores matrix and macropores. The macropores or air pores, with radius of 50–1000 μm, are formed due to the expansion of the mass caused by the foaming agent. Micropores appear in the walls between the macropores and they are divided in macrocapillaries of 50 nm to 50 μm and microcapillaries of 50 nm or less [14, 15]. It can also be seen two main typologies of pores: closed and open pores. Closed pores are isolated from the external surface and open pores are connected to the external surface and are therefore accessible to liquids and gases. Open pores can be further

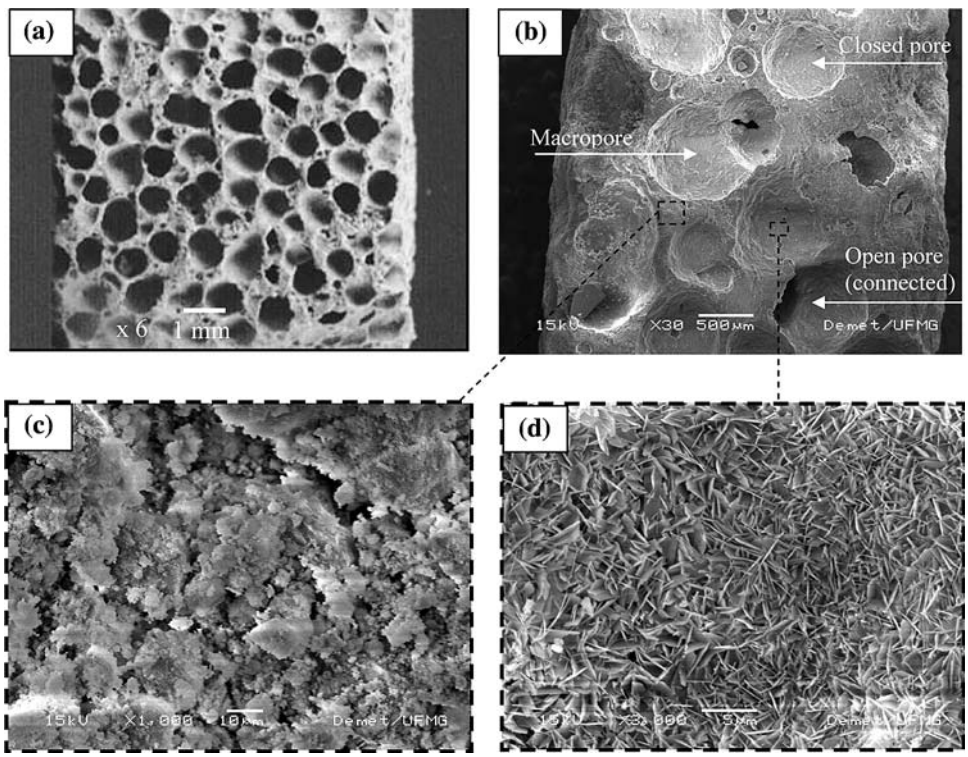

Fig. 2 **a** Typical pore structure obtained for the 3D scaffolds under evaluation; **b** macropores; **c** macrocapillaries; **d** microcapillaries

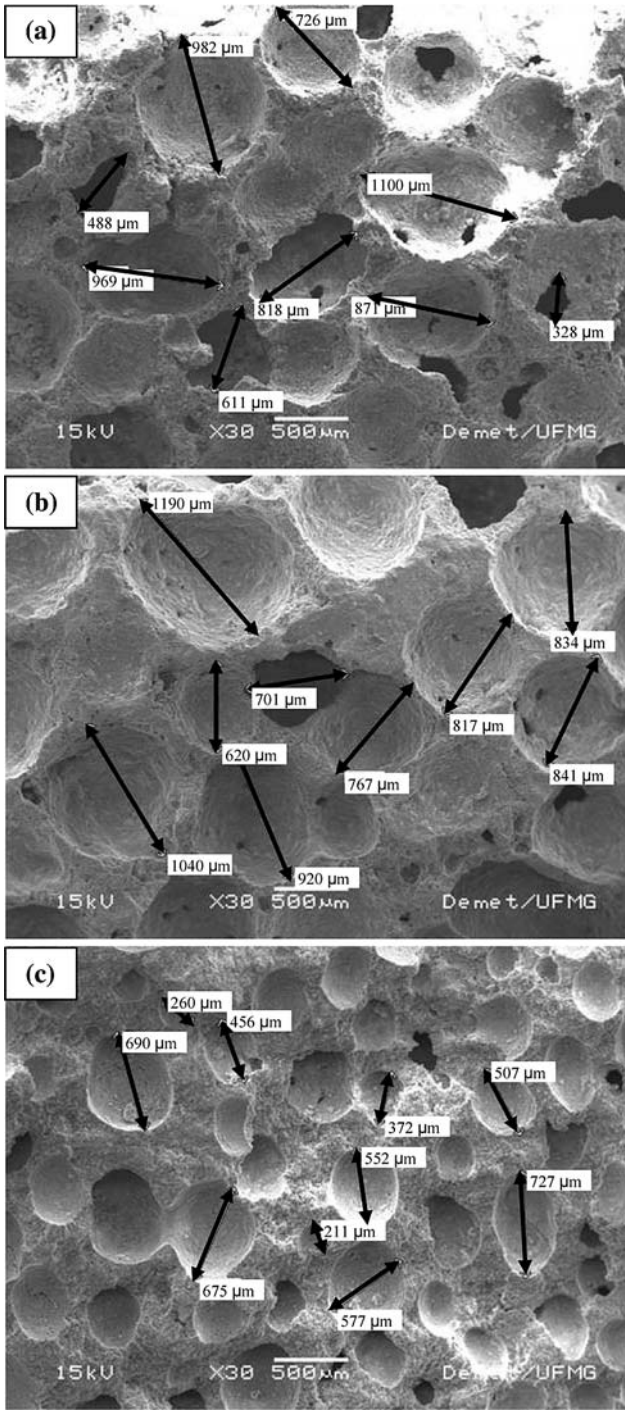

Fig. 3 The macrostructure of analyzed specimens (SE, 30×): **a** R1_NA (quartz and air curing); **b** R1_A (quartz and autoclaving); **c** R2_NA (silica fume and air curing)

divided in dead-end or interconnected pores. It is interesting to note that the closed macropores of the scaffolds may not be real closed pores. They are isolated from the external surface but can be connected via micropores intermediaries. A more in-depth evaluation of porosity would require sequential cross-sections.

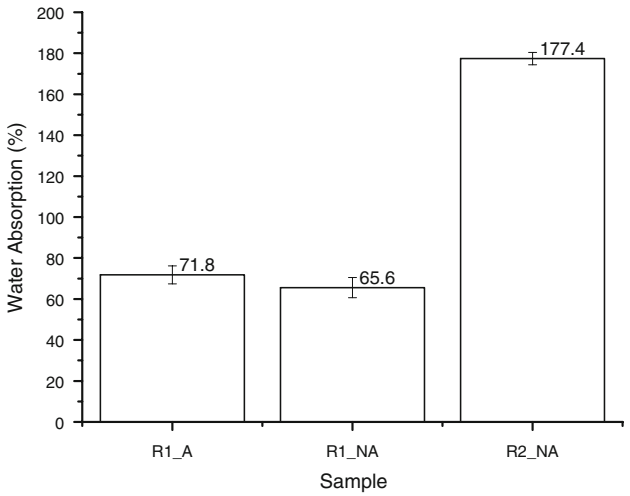

Fig. 4 Water absorption results for scaffolds with different processing parameters

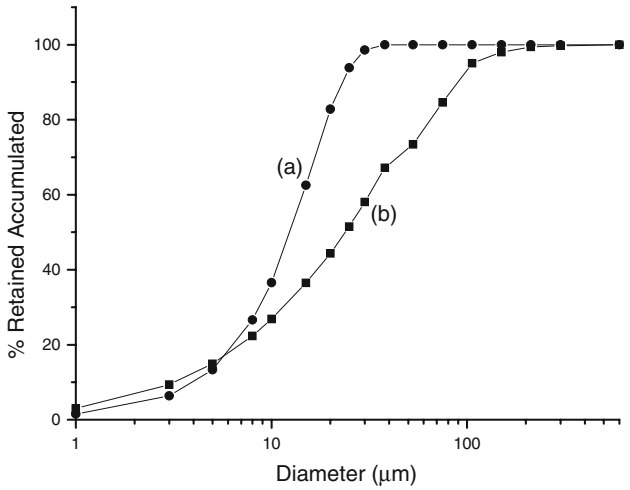

Fig. 5 Particle size distribution for sílica fume (a) and ball-milled quartz (b) obtained using CILAS Laser Diffraction Particle Size Analysis Instrument

Examination of the ruptured surfaces by scanning electron microscopy revealed that substrates produced by R1 (Fig. 3a, b) are obtained with an interconnected porous network and open macropores ranging from 300–1,100 µm. For R2 samples (Fig. 3c), air pores are relatively less connected with radius of 200–750 µm. The results favor the use of the scaffolds under evaluation as repairing biomaterial once for colonization of the pores by bone tissue to take place pores should be larger than 50 µm [1, 16]. Also, the large pore size (200–1,100 µm) of scaffolds enhances the diffusion of nutrients to the 3D substrates and medium exchange [5].

Water absorption is among the main techniques used to measure porosity [17] which influences some important properties of scaffolds such as strength, tissue intergrowth, and vascularization [5, 16]. Figure 4 shows the water

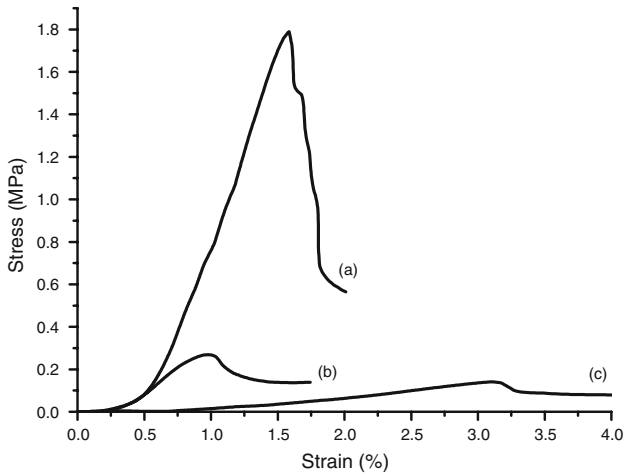

Fig. 6 Typical Stress × Strain curves obtained for the scaffolds under evaluation: (a) R1_A (quartz and autoclaving), (b) R1_NA (quartz and air curing), and (c) R2_NA (silica fume and air curing)

absorption for the scaffolds prepared with different processing parameters. The substrate prepared using R2 presented highly porous structure when compared to R1 materials, independent of curing method. These results highlighted the major direct role of capillary porosity on water absorption. As it can be seen in Figs. 3 and 4, sample R2_NA presented lesser macropores volume, resulting in higher contribution from cement matrix phase, and higher absorption when compared to substrates obtained via R1. Water absorption has raised by changing from quartz to silica fume as a consequence of the increase of water needed for achieving a workable and stable mix with this material. A relatively higher water: solids ratio produces a weaker and pervious matrix, leading to a higher capillary porosity which is in turn responsible for increasing of water absorption of pastes with silica fume [14]. The higher water demand of this compound is associated with its fineness higher than that of ball-milled quartz (Fig. 5).

Compressive strength properties (Fig. 6) reflected the water absorption previous results and cement hydration products formed as a consequence of the different curing methods (air curing or autoclaving) evaluated using XRD technique (Figs. 7 and 8). The compressive strength of R1_A reached (1.89 ± 0.33) MPa while for R1_NA and R2_NA samples values of (0.23 ± 0.04) MPa, and (0.14 ± 0.02) MPa were obtained, respectively. Modulus of elasticity was qualitatively estimated through Stress × Strain curves. The trend regarding to modulus of elasticity value was crescent in the same order measured for compressive property: R2_NA < R1_NA < R1_A. This result is in agreement with literature for aerated cement materials which reports that modulus of elasticity in compression is a direct function of the compressive strength [15].

The decrease of compressive strength with increasing porosity was not surprising and such trend has been reported elsewhere by various authors [16, 18]. It is related to the reduction in the quantity of solid material present in each specimen. This feature can explain the difference of mechanical resistance from samples R1 when compared to R2.

However, for samples obtained through R1, which possess pore systems largely identical, the differences in the mechanical properties of R1_A when compared to R1_NA were caused by the variation in the hydration

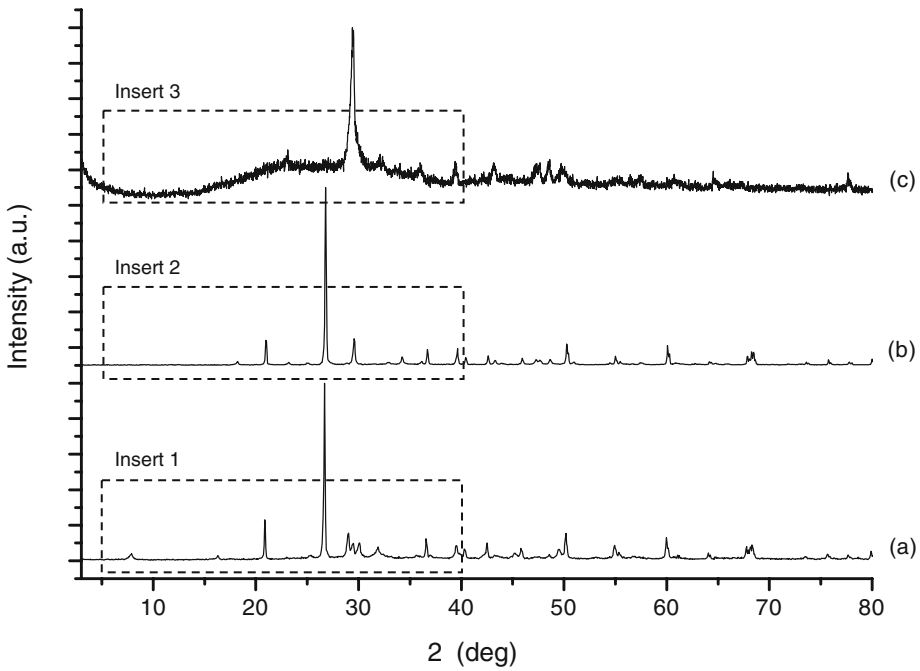

Fig. 7 X-ray diffractograms for (a) R1_A (quartz and autoclaving), (b) R1_NA (quartz and air curing) and (c) R2_NA (silica fume and air curing) scaffolds

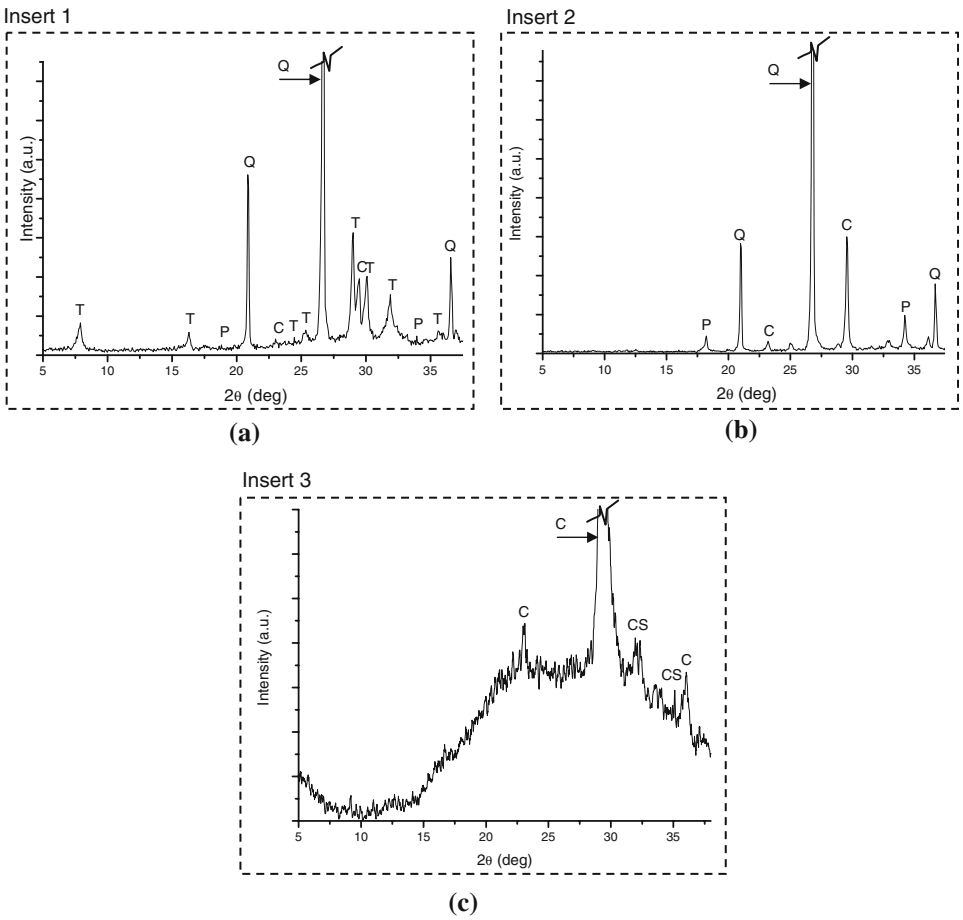

Fig. 8 Inserts from diffractograms for **a** R1_A (quartz and autoclaving), **b** R1_NA (quartz and air curing), and **c** R2_NA (silica fume and air curing) showing crystalline phases identified for each prepared scaffolds (CS = anhydrous calcium silicate; P = Portlandite; Q = Quartz; C = Calcite; T = Tobermorite)

products. Autoclaving increases the compressive strength significantly, as high temperature and pressure result in a stable form of tobermorite [15]. Under autoclave conditions, the solubility of SiO_2 is increased whilst the solubility of CaO is decreased. All the dissolved SiO_2 reacts chemically with available CaO forming the microcrystalline structure of tobermorite ($5CaO \cdot 6SiO_2 \cdot 5H_2O$) with much lower specific surface and a Ca/Si ratio approximately equal to 0.83 [15, 19, 20]. On air cured conditions, the Portland cement hydration product is also a calcium silicate hydrate (C–S–H), but due to the higher solubility of $Ca(OH)_2$ in comparison to the siliceous material at ambient temperature, a Ca-rich C–S–H is formed (Ca/Si $\sim$ 1.7–2.0), with a lower degree of polymerization of the chains (practically amorphous C–S–H), accompanied by a very high pH of pore solution [20, 21]. All these features are demonstrated in the XRD patterns obtained for the samples under evaluation shown in details in Fig. 8. In the diffractograms it is clear the tobermorite formation under autoclaving cure and the higher amount of $Ca(OH)_2$, portlandite, available in air cured scaffolds. It is important to pointed out that this former compound leads to a high pH value in the surrounding environment of application, which can be detrimental to cells [5, 6].

Figure 9 shows de FTIR spectra from the anhydrous Portland cement (a) used for substrates preparation and from scaffolds R1_NA (b) and R1_A (c). The spectrum of anhydrous cement clearly revealed the major peak of

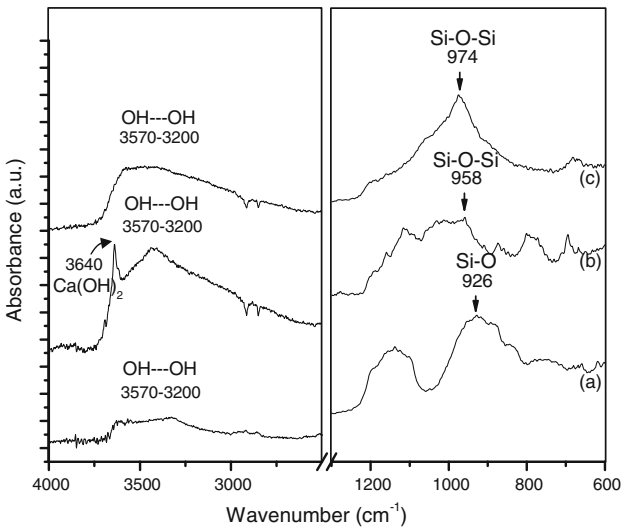

Fig. 9 FTIR spectra from (a) Portland cement, (b) R1_NA (air cured), and (c) R1_A (autoclaved)

calcium silicates due to Si–O asymmetric stretching vibration ($v_3 = 926\ cm^{-1}$) [22–24]. This peak underwent changes during hydration, the most evident being its shifting to higher wavenumber. This shifting indicates polymerization of the silicate units ($(SiO_4)^{4-}$) and it is considered a fingerprint evidence for degree of polymerization with the formation of C–S–H phase [22]. Based on FTIR spectra, the degree of polymerization of cured samples was different, with the R1_A scaffold presenting a higher degree of polymerization of Si–O–Si chains than R1_NA, endorsing the formation of a more organized phase (tobermorite) under autoclaving, as previously discussed.

The spectral data changes upon air cure (Fig. 9b) have also indicated the formation of portlandite by the presence of the peak at 3,640 cm^{-1}, due to the OH^- band from $Ca(OH)_2$, which was not observed in the scaffold treated at high temperature and pressure (Fig. 9c), supporting XRD results. The broad band on both substrates in the range from 3,570 to 3,200 cm^{-1} is related to symmetric and asymmetric (v_1 and v_3) stretching vibrations of OH^- adsorbed water molecules attributed to cement hydration [22, 23].

Based on the results of XRD and FTIR, a comparison between autoclaving versus air curing can be summarized in a relative simple way (some processes are until today not fully scientifically understood) in Eqs. 3 and 4. In these equations, CaO compound is supplied by cement and lime and SiO_2 is a constituent of cement and silica sand. According to Eq. 3, autoclaving creates a well crystallized calcium silicate hydrate, more specifically tobermorite, consequence of hydrothermal processing conditions and the presence of other compounds (aluminates and sulfates). On the other hand (Eq. 4), air curing hydration products are mainly poorly crystallized or amorphous calcium silicate hydrates and portlandite.

The overall result of the investigated properties indicates that only the scaffold R1_A have presented compressive resistance comparable to that of human bone and bioceramics porous scaffolds used as bone substitutes. Bone tissues differ in their amounts of porosity, mineralization, reconstruction, and preferred orientation. All these have important effects on mechanical properties. Very porous, trabecular bone is always weaker and more compliant than compact bone on a weight basis, yet it occurs in places where its energy absorbing ability, or its low density, is advantageous. As a reference, considering donor age, gender, among several other factors, the range expected for ultimate stress is from 0.2 to 15 MPa in trabecular bone when evaluated by compressive mechanical test [2, 5, 25]. On the other hand, the properties of cortical bone may approach 150 MPa [26]. Compressive strength of tri-dimensional porous HA structures have been reported in the literature from 0.3 to 5.0 MPa [2]. Based strictly on the mechanical properties reported, one may assume that the R1_A (quartz sand and autoclaved) scaffold developed in the present work is suitable for partial replacement of damaged trabecular (cancellous) bone tissue.

$$x\mathrm{CaO} + y\mathrm{SiO_2} + z\mathrm{H_2O} \xrightarrow{\text{Autoclave, 160-190°C, 1200-1300 KPa}} \text{Tobermorite } (5\mathrm{CaO}\cdot 6\mathrm{SiO_2}\cdot 5\mathrm{H_2O}) \quad (3)$$

$$x\mathrm{CaO} + y\mathrm{SiO_2} + z\mathrm{H_2O} \xrightarrow{\text{Air cured}} \text{C-S-H} + \text{Portlandite } (\mathrm{Ca(OH)_2}) + \text{Silica sand } (\mathrm{SiO_2}) \quad (4)$$

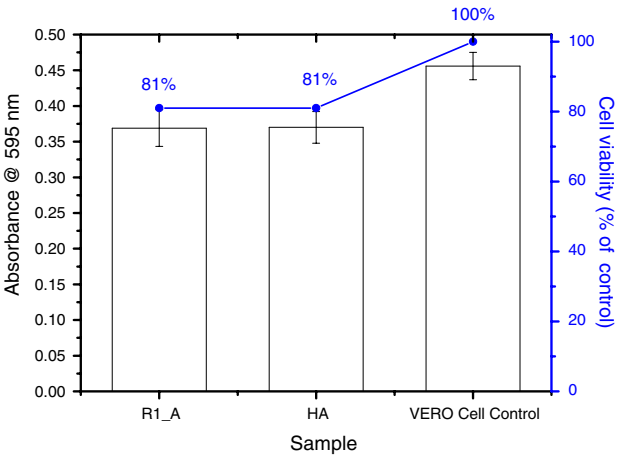

Fig. 10 Relative cell viability of VERO cells seeded onto R1_A sample and HA

3.2 Cytocompatibility, cell viability and bioactivity assays

Safety tests including cytotoxicity analysis are required for all products to be used in contact with human and animals. Cytotoxicity tests using cell cultures have been accepted as the first step in identifying active compounds and for biosafety testing.

The cell viability for the scaffold selected based on mechanical properties (R1_A) assessed by the MTT assay is presented in Fig. 10. The cells seeded onto autoclaved porous structure as prepared showed good cell viability compared to the control (cell culture) and to HA used as a widely accepted biomaterial of reference.

Moreover, VERO cell spreading and adhesion test on the developed Portland cement scaffolds were used as the evaluation assay of the cytotoxicity and biocompatibility of samples. Cell spreading was primarily assessed by SEM examination of the sample as shown in Fig. 11.

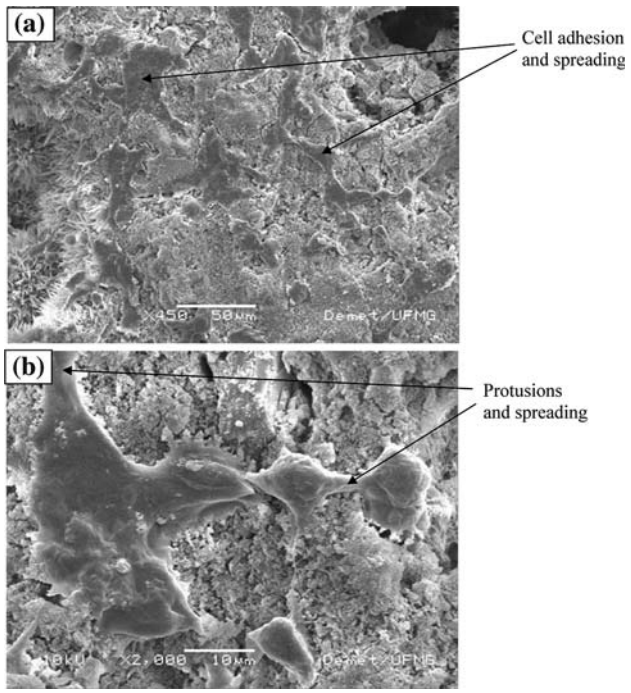

Fig. 11 VERO cells spreading and attachment assays. SEM photomicrograph of cell spreading and adhesion on Portland cement macroporous substrate (**a** and **b**)

Cell adhesion is involved in various natural phenomena such as embryogenesis, maintenance of tissue structure, wound healing, immune response, metastasis, and tissue integration of biomaterials [27]. Since cellular attachment, adhesion, and spreading belong to the first phase of cell/material interactions, the quality of this phase will influence proliferation and differentiation of cells on biomaterials surfaces. Based on the SEM images, cells spreading and attachment were clearly verified on R1_A macroporous structure.

According to the literature [27–29], cell spreading are usually divided into three main interaction levels: (a) not spread: cells were still spherical in appearance, protrusions or lamellipodia were not yet produced; (b) partially spread: at this stage, cells began to spread laterally at one or more sides, but the extensions of plasma membrane were not completely confluent; and (c) fully spread. The last model (c) would represent the best result for material cell hosting and it was verified for R1_A material. The cells on the scaffolds underwent their morphological changes to stabilize the cell-biomaterial interface. They spread and established close contact with the material adapting a flattened morphology and showing numerous filopodia anchoring the cells to the substrate.

Based on that, the 3D macroporous Portland cement scaffold produced in this study has proven to be biocompatible and with high potential for cell culture and growth. Such behavior is supported by previous studies which have indicated the biocompatibility of calcium silicate ceramics after deposition of an apatite-like layer. For materials based on hydrated calcium silicates, carbonation and/or mixtures using pozzolanic agents have resulted in some biocompatible substrates. In this work, the outstanding biocompatibility verified is assumed to be related to the tobermorite formation by autoclaving process, which optimizes the pH value of the system to physiological levels, suitable for cell growth, overcoming the main drawback associated with bone substitutes based on Portland cement.

4 Conclusions

Highly porous interconnective scaffolds with a pore size ranging from 300–1,100 μm were successfully prepared using Portland cement and lime as binders and metallic aluminum as porogen agent. Mechanical strength in the range suitable for repairing trabecular bones was produced due to tobermorite formation by autoclave curing. Tobermorite as main phase of Portland cement hydration was also responsible for the observed biocompatibility as a consequence of physiological pH attained with this compound. The developed process has opened a window of opportunity on a promising alternative route for producing 3D biomaterials to be used in bone tissue engineering.

Acknowledgments The authors acknowledge financial support from CNPq/FAPEMIG. Also we are grateful to Laboratory of Ceramic Materials (Prof. Wander L. Vasconcelos), Laboratory of Electron Microscopy (Prof. Dagoberto B. Santos and Patrícia M. T. de Azevedo), Laboratory of X-Ray Diffraction (Prof. Vicente T. L. Buono e Andréia B. Henriques), and Laboratory of Microbiology (Prof. Edel F. Barbosa-Stancioli).

References

1. H.S. Mansur, H.S. Costa, A.A.P. Mansur, M.M. Pereira, E.F. Barbosa-Stancioli, J. Mater. Sci. **43**, 510 (2008). doi:10.1007/s10853-007-1849-6
2. H.S. Mansur, H.S. Costa, G.I. Andrade, M.M. Pereira, E.F. Barbosa-Stancioli, J. Mater. Res. **10**, 21 (2007)
3. F.D. Beaman, L.W. Bancroft, J.J. Peterson, M.J. Kransdorf, Radiol. Clin. North Am. **44**, 451 (2006). doi:10.1016/j.rcl.2006.01.001
4. D.W. Hutmacher, Biomat **21**, 2529 (2000). doi:10.1016/S0142-9612(00)00121-6
5. C. Wu, Y. Ramaswamy, P. Boughton, H. Zreiqat, Acta. Biomater. **4**, 343 (2008). doi:10.1016/j.actbio.2007.08.010
6. D. Gallego, N. Higuita, F. Garcia, N. Ferrell, D.J. Hansford, Mater. Sci. Eng. C **28**, 347 (2008). doi:10.1016/j.msec.2007.04.020
7. Z. Gou, J. Chang, W. Zhai, J. Eur. Ceram. Soc. **25**, 1507 (2005). doi:10.1016/j.jeurceramsoc.2004.05.029
8. N. Higuita, D. Gallego, F. Garcia, D. Hansford, in *Proceedings of II Colombian Congress of Bioengineering and Biomedical Engineering*, Colômbia, 2005, p. 1

9. W. Zhao, J. Wang, W. Zhai, Z. Wang, J. Chang, Biomat **26**, 6113 (2005). doi:10.1016/j.biomaterials.2005.04.025
10. H. Engqvist, J.-E. Schultz-Walz, J. Loof, G.A. Botton, D. Mayer, M.W. Phaneuf et al., Biomat **25**, 2781 (2004). doi:10.1016/j.biomaterials.2003.09.053
11. H.F.W. Taylor, *Cement Chemistry*, 2nd edn. (Thomas Telford, London, 1997), pp. 113–116
12. C.C.D. Coumes, S. Courtois, D. Nectoux, S. Leclercq, X. Bourbon, Cem. Concr. Res. **36**, 2152 (2006). doi:10.1016/j.cemconres.2006.10.005
13. M. Venuat, *Aditivos y tratamientos de morteros y hormigones*, 1st edn. (Editores Tecnicos Asociados S.A, Barcelona, 1972)
14. E.K.K. Nambiar, K. Ramamurthy, Cem. Concr. Res. **37**, 1341 (2007). doi:10.1016/j.cemconres.2007.05.010
15. N. Narayanam, K. Ramamurthy, Cem. Concr. Compos. **22**, 321 (2000). doi:10.1016/S0958-9465(00)00016-0
16. J.C. Le Huec, T. Schaeverbeke, D. Clement, J. Faber, A. Le Rebeller, Biomat **16**, 113 (1995). doi:10.1016/0142-9612(95)98272-G
17. F. Andreola, C. Leonelli, M. Romagnoli, P. Miselli, Ceram. Bull. **79**, 49 (2000)
18. K. de Groot, in *Bioceramics of Calcium Phosphate*, ed. by K. de Groot (CRC Press, Boca Raton, 1983), p. 99
19. S.Y. Hong, F.P. Glasser, Cem. Concr. Res. **34**, 1529 (2004). doi:10.1016/j.cemconres.2003.08.009
20. T. Dietz, K. Bohnemann, in *Proceedings of 7th International Inorganic-Bonded Wood & Fiber Composite Materials Conference*, Sun Valley, 2000, p. 13
21. F. Merlin, J. Mater. Chem. **12**, 3308 (2002). doi:10.1039/b205279m
22. M.Y.A. Mollah, W. Yu, R. Schennach, D.L. Cocke, Cem. Concr. Res. **30**, 267 (2000). doi:10.1016/S0008-8846(99)00243-4
23. M. Yousuf, A. Mollah, P. Palta, T.R. Hess, R.K. Vempati, D.L. Cocke Cem, Concr. Res. **25**, 671 (1995). doi:10.1016/0008-8846(95)00055-H
24. V.C. Farmer, *The Infrared Spectra of Minerals* (Adlard & Son Ltd, London, 1974), pp. 445–463
25. A.S.P. Lin, T.W. Barrows, R.E. Guldberg in *Proceedings of 2001 Bioengineering Conference, ASME*, Salt Lake City, 2001, p. 203
26. D.T. Reilly, A.H. Burstein, J. Bone. Jt. Surg. **56A**, 1001 (1974)
27. S. Hannah, S.I. Samuel, Biomat **26**, 5492 (2005). doi:10.1016/j.biomaterials.2005.01.043
28. S. Bose, J. Darsell, H.L. Hosick, L. Yang, D.K. Sarkar, A. Bandyopadhyay, J. Mater. Sci. Mater. Med. **13**, 23 (2002). doi:10.1023/A:1013622216071
29. G.A. Dunn, D. Zicha, J. Cell. Sci. **108**, 1239 (1995)